Na+-dependent phosphate transporters in the murine osteoclast: cellular distribution and protein interactions

Mohammed A. Khadeer, Zhihui Tang, Harriet S. Tenenhouse, Maribeth V. Eiden, Heini Murer, Natividad Hernando, Edward J. Weinman, Meenakshi A. Chellaiah and Anandarup Gupta

Am J Physiol Cell Physiol 284:1633-1644, 2003. First published Feb 26, 2003;
doi:10.1152/ajpcell.00580.2002

Am J Physiol Cell Physiol 284: C1633–C1644, 2003.
First published February 26, 2003; 10.1152/ajpcell.00580.2002.

Na^+-dependent phosphate transporters in the murine osteoclast: cellular distribution and protein interactions

Mohammed A. Khadeer,[1]* Zhihui Tang,[1]* Harriet S. Tenenhouse,[2] Maribeth V. Eiden,[3] Heini Murer,[4] Natividad Hernando,[4] Edward J. Weinman,[5] Meenakshi A. Chellaiah,[1] and Anandarup Gupta[1]

[1]*Department of Oral and Craniofacial Biological Sciences, University of Maryland, Baltimore, Maryland 21201;* [2]*Departments of Pediatrics and Human Genetics, Montreal Children's Hospital Research Institute, McGill University, Montreal, Quebec, Canada H3Z 2Z3;* [3]*Laboratory of Cellular and Molecular Regulation, National Institute of Mental Health, Bethesda, Maryland 20892;* [4]*Physiologisches Institut, Universität Zürich-Irchel, Zürich, CH-8057, Switzerland; and,* [5]*Department of Medicine, University of Maryland, Baltimore, Maryland 21201*

Submitted 12 December 2002; accepted in final form 21 February 2003

Khadeer, Mohammed A., Zhihui Tang, Harriet S. Tenenhouse, Maribeth V. Eiden, Heini Murer, Natividad Hernando, Edward J. Weinman, Meenakshi A. Chellaiah, and Anandarup Gupta. Na^+-dependent phosphate transporters in the murine osteoclast: cellular distribution and protein interactions. *Am J Physiol Cell Physiol* 284: C1633–C1644, 2003. First published February 26, 2003; 10.1152/ajpcell.00580.2002.—We previously demonstrated that inhibition of Na-dependent phosphate (P_i) transport in osteoclasts led to reduced ATP levels and diminished bone resorption. These findings suggested that Na/P_i cotransporters in the osteoclast plasma membrane provide P_i for ATP synthesis and that the osteoclast may utilize part of the P_i released from bone resorption for this purpose. The present study was undertaken to define the cellular localization of Na/P_i cotransporters in the mouse osteoclast and to identify the proteins with which they interact. Using glutathione *S*-transferase (GST) fusion constructs, we demonstrate that the type IIa Na/P_i cotransporter (Npt2a) in osteoclast lysates interacts with the Na/H exchanger regulatory factor, NHERF-1, a PDZ protein that is essential for the regulation of various membrane transporters. In addition, NHERF-1 in osteoclast lysates interacts with Npt2a in spite of deletion of a putative PDZ-binding domain within the carboxy terminus of Npt2a. In contrast, deletion of the carboxy-terminal TRL amino acid motif of Npt2a significantly reduced its interaction with NHERF-1 in kidney lysates. Studies in osteoclasts transfected with green fluorescent protein-Npt2a constructs indicated that Npt2a colocalizes with NHERF-1 and actin at or near the plasma membrane of the osteoclast and associates with ezrin, a linker protein associated with the actin cytoskeleton, likely via NHERF-1. Furthermore, we demonstrate by RT/PCR of osteoclast RNA and in situ hybridization that the type III Na/P_i cotransporter, PiT-1, is also expressed in mouse osteoclasts. To examine the cellular distribution of PiT-1, we infected mouse osteoclasts with a retroviral vector encoding PiT-1 fused to an epitope tag. PiT-1 colocalizes with actin and is present on the basolateral membrane of the polarized osteoclast, similar to that previously reported for Npt2a. Taken together, our data suggest that association of Npt2a with NHERF-1, ezrin, and actin, and of PiT-1 with actin, may be responsible for membrane sorting and regulation of these Na/P_i cotransporters in the osteoclast.

phosphate transport; osteoclasts; Npt2a; NHERF-1; PiT-1

PHOSPHATE (P_i) is the major anionic component of the mineralized bone matrix (2). Previously, we had hypothesized that during the process of bone resorption, part of the P_i released from bone may be utilized by the osteoclast to maintain cellular ATP content during the cyclical processes of migration, attachment, and resorption (10). In addition, we provided evidence for the expression of the type II family of Na/P_i cotransporters in the osteoclast, identical or closely related to the type IIa cotransporter (Npt2a) in the renal proximal tubule (11). The Npt2a protein mediates the rate-limiting step in renal P_i reabsorption (27). The importance of Npt2a in the regulation of extracellular P_i was suggested by recent studies in which the *Npt2a* gene was inactivated in mice by targeted mutagenesis (3). Previously, we examined the impact of *Npt2a* gene ablation on the skeletal phenotype in mice. At weaning, *Npt2a*−/− mice showed several skeletal abnormalities, including retarded secondary ossification, increased trabecular thickness, retention of growth plate proteoglycan in trabecular bone, and a reduction in osteoclast number. However, with increasing age, there was a correction of the skeletal phenotype (11).

We demonstrated that the Npt2a-immunoreactive protein is localized exclusively on the basolateral membrane (BLM) and in areas contiguous to the sealing zone of the polarized osteoclast (10). Disruption of the actin cytoskeleton in polarized osteoclasts with cytochalasin D inhibited P_i uptake by ~80% (10). Because Na/P_i cotransport in the osteoclast is regulated by the actin cytoskeleton, we hypothesized that the

*M. A. Khadeer and Z. Tang contributed equally to this work.

Address for reprint requests and other correspondence: A. Gupta, Dept. of Oral and Craniofacial Biological Sciences, Univ. of Maryland, 666 West Baltimore St., Baltimore, MD 21201 (E-mail: ang001@dental.umaryland.edu).

The costs of publication of this article were defrayed in part by the payment of page charges. The article must therefore be hereby marked "*advertisement*" in accordance with 18 U.S.C. Section 1734 solely to indicate this fact.

Npt2a-immunoreactive protein in the osteoclast associates indirectly with the actin cytoskeleton and that this interaction may be a determinant of the plasma membrane localization and activity of Npt2a in the osteoclast.

The first aim of the present study was to identify a linker protein that would provide a bridge between the actin cytoskeleton and the Npt2a protein. In the kidney, Gisler et al. (9) identified a protein-binding V/ATXL domain in the COOH terminus of the Npt2a protein, representing a potential PDZ (PSD-95/Dlg/ZO-1)-interacting motif. PDZ domains are conserved protein modules that mediate protein-protein interactions associated with the plasma membrane (7). One such PDZ protein, Na/H exchanger regulatory factor (NHERF-1), has been found to participate in regulation of phosphorylation, targeting, endocytic retrieval, and trafficking of several membrane transporters, including Npt2a in the kidney (9, 26). In the present study, we undertook to determine whether the Npt2a protein also associates with NHERF-1 in the osteoclast, because this association may play a role in the cellular localization of Npt2a.

Previous studies have shown that Npt2a knockout (*Npt2a*−/−) mice exhibit an age-dependent increase in type III Na/P_i cotransporter mRNA expression in the kidney as part of an effort to compensate for the loss of the *Npt2a* gene (12). We hypothesized that the expression and regulation of the type III family of Na/P_i cotransporters in the osteoclast could account for reversal of the skeletal phenotype in the *Npt2a*−/− mice (11). Thus, in the present study, we sought to examine the expression and cellular localization of the type III family of Na/P_i cotransporters in murine osteoclasts. The type III Na/P_i cotransporters, originally identified as retroviral receptors for the gibbon ape leukemia virus (galv), are ubiquitously expressed and thought to function as housekeeping Na/P_i cotransporters (14, 15). One such galv receptor, PiT-1 (also known as Glvr-1), is expressed at high levels in bone marrow, osteoblasts, and chondrocytes (21, 23).

Our study suggests that association of Npt2a with a PDZ protein such as NHERF-1, and of PiT-1 with actin, may play a role in membrane sorting and regulation of these Na/P_i cotransporters in the osteoclast.

MATERIALS AND METHODS

Reagents. The enhanced green fluorescent protein (EGFP)-Npt2a constructs encoding for the wild type (WT) and COOH-terminal TRL deletions (Npt2a-ΔTRL) were prepared as previously described (13). Briefly, the mouse type IIa (mIIa) Na/P_i cotransporters were fused to the COOH terminus of the EGFP by inserting the Npt2a (−WT and −ΔTRL) cDNAs into the pEGFP-C1 vector. Dr. Vijaya Ramesh (Molecular Neurogenetics Unit, Massachusetts General Hospital, Charlestown, MA) provided the glutathione *S*-transferase (GST)-NHERF-1 fusion protein. A rabbit osteoclast cDNA library was the gift of Dr. M. Kumegawa (Meikai University, Sakado, Japan) (28). The murine macrophage (mMa) cDNA library was obtained from Stratagene (La Jolla, CA). Recombinant osteoprotegerin ligand (OPGL) was prepared as previously described (5). Most reagents were of analytical grade and were purchased from Sigma (St. Louis, MO) unless otherwise indicated.

Mice. Mice (C57BL/6NHsd, 6–7-wk-old) were purchased from Harlan (Indianapolis, IN). *Npt2a* knockout mice were established by homologous recombination (3). Wild-type (*Npt2a*+/+) and homozygous mutant (*Npt2a*−/−) mice, generated by crossing heterozygous (*Npt2a*+/−) male and female mice, were genotyped by PCR amplification of genomic DNA as previously described (3).

Murine osteoclast culture. The tibiae and femurs of 7-wk-old mice were used to isolate bone cells, as previously described (4, 11). Bone marrow cells were suspended in α-minimal essential medium (αMEM, GIBCO-BRL) supplemented with 10% fetal bovine serum (α-10 MEM) and cultured at 37°C in a 5% CO_2 incubator. After 24 h, nonadhered cells were layered on Histopaque-1077 (Sigma) and centrifuged at 300 *g* for 15 min at room temperature. The cell layer between the Histopaque and the medium was removed and washed with α-10 MEM and then centrifuged at 2,000 rpm for 7 min. mCSF-1 (R & D Systems, Minneapolis, MN) was added to the cultures at a concentration of 10 ng/ml, and OPGL was added at 50–100 ng/ml. The multinucleated osteoclasts were seen to form and mature after *day 4*. Their viability was routinely assessed by trypan blue dye exclusion, and the percentage of tartrate-resistant acid phosphatase (TRAP)-positive cells was assessed to be ~99%, as previously described (11).

Preparation of the GST-Npt2a fusion proteins. EGFP-Npt2a constructs, encoding the WT and COOH-terminal TRL deletion (ΔTRL) cDNAs, were prepared as previously described (13). These constructs served as templates for generation of the GST-Npt2a-WT and GST-Npt2a-ΔTRL fusion proteins. Npt2a-WT and Npt2a-ΔTRL fragments were PCR amplified by using the following primers: WT *Npt2a*: forward, 5′-CCGGAATTCATGTCCTGCAGAGCCGAA-3′, and reverse, 5′-CCGCTCGAGTAGAGGCGGGTAGCATT-3′; *Npt2a-ΔTRL*: forward, 5′-CCGGAATTCATGTCCTGCAGAGCCGAA-3′, and reverse, 5′-CCGCTCGAGTAGCATTGTGGTGAGCAG-3′. Amplification was carried out using a hot start method and *Taq* DNA polymerase (Life Technologies) with denaturation at 94°C for 1 min, annealing at 50°C for 1 min, and extension at 72°C for 1 min. At the end of 35 cycles, an extension cycle for 10 min at 72°C was performed. Both the Npt2a-WT (82 amino acids, 246 bp) and the Npt2a-ΔTRL (79 amino acids, 234 bp) fragments were directionally cloned into pGEX-5X-1 (Amersham Biosciences, Piscataway, NJ) at the *EcoR*1 and *Xho*1 sites. Positive clones were identified and confirmed by sequencing with pGEX-5′ end primer. Subsequently, these clones were transformed in BL-21 cells. The GST-NHERF-1 (1–358 amino acids) fusion protein was provided in a pGex/BL21 construct by Dr. Vijaya Ramesh and was purified using a similar protocol.

Purification of GST-Npt2a fusion proteins. Overnight cultures of both the recombinant GST-Npt2a in BL-21 cells were transferred into larger volumes of LB/Amp, grown for 2 h until the OD_{600} was determined to be 1.0, and subsequently induced with 1.0 mM isopropyl-β-D-thiogalactopyranoside (IPTG) for an additional 2 h at 37°C. Thereafter, the cultures were spun down at 2,500 rpm for 20 min. The pellets were resuspended in 3.6 ml of binding buffer that comprised 50 mM Tris-Cl, pH 8.0, 120 mM NaCl, 0.5% NP-40, 1 mM dithiothreitol (DTT), 1 mM phenylmethylsulfonyl fluoride (PMSF), and a protease inhibitor cocktail (Roche Diagnostics, Mannheim, Germany). Then, 0.4 ml of lysozyme (10 μg/ml) was added, and the mixture was allowed to stand at room temperature for 20 min. The bacteria were lysed by repeated freeze-thaw cycles. The lysates were centrifuged at 14,000 rpm for 20 min. The supernatants were collected (~4 ml) and

incubated with 200 μl of washed GST-Sepharose; these were rocked at room temperature for 1 h. The Sepharose beads were washed five times for 10 min each using 10 volumes of binding buffer. An aliquot of ~10 μl of GST-bound proteins was taken and separated on 8% SDS-PAGE. After the extraction was confirmed, a 50% suspension of this extract was prepared with binding buffer and stored at 4°C.

Preparation of kidney homogenate and osteoclast cell lysates. Kidneys were homogenized in lysis buffer (10 mM Tris-Cl, pH 7.6, 150 mM NaCl, 1% NP-40, 10% glycerol plus protease inhibitor cocktail) for 1 h at 4°C. Osteoclast cell lysates were prepared in modified RIPA buffer (10 mM Tris-Cl, pH 7.4, 150 mM NaCl, 0.5% Triton X-100, 1% deoxycholic acid, 0.1% SDS, and 1% NP-40). The cells were spun down at 14,000 rpm at 4°C for 10 min. The supernatants were collected and bound to fusion proteins as detailed below.

GST-sepharose and nickel-agarose affinity-precipitation assays. To perform affinity-precipitation of NHERF-1, GST-beads (Qiagen, Valencia, CA) bound to fusion proteins (Npt2a-WT or Npt2a-ΔTRL) or GST (control) were incubated with either (~500 μg) murine osteoclast or rat kidney (~100 μg) lysates at 4°C for 2–4 h. The beads were pelleted at 500 *g* for 2 min, washed four times with binding buffer, resuspended in 1–2 volumes of sodium dodecyl sulfate (SDS)-polyacrylamide gel electrophoresis (PAGE) sample buffer, and boiled before fractionation on SDS-PAGE. The proteins were then transferred to polyvinylidene difluoride membranes (PVDF; Bio-Rad Laboratories, Hercules, CA) for Western analyses with a polyclonal antibody to NHERF-1 at a dilution of 1:1,000. A similar protocol was followed for incubation of murine osteoclast lysates with the GST-NHERF-1 fusion protein for affinity-precipitation of Npt2a. For the nickel (Ni)-agarose affinity-precipitation assays, the following conditions were used: Ni-agarose (Qiagen, Valencia, CA) beads (15 μl) were incubated with 500 μl of the 6XHis-tagged NHERF-1 fusion protein (0.2 mg/ml) for 1 h and subsequently incubated with ~500 μg of murine osteoclast lysates overnight at 4°C. The beads were washed with washing buffer (50 mM NaH_2PO_4, 300 mM NaCl, 20 mM imidazole, pH 8.0) three times for 10 min each. The beads were collected after centrifugation at 500 *g* for 2 min. Elution buffer (20 μl, 50 mM NaH_2PO_4, 300 mM NaCl, 250 mM imidazole, pH 8.0) was added and incubated at 4°C for 1 h. The negative control for the Ni-agarose affinity-precipitation was performed by incubating osteoclast lysates with Ni-agarose beads alone in the absence of the 6XHis-tagged NHERF fusion protein. SDS-sample buffer was added to the beads and boiled, and the affinity precipitates were separated on SDS-PAGE. After transfer to PVDF membranes, the blots were probed with a polyclonal antibody to Npt2a at a 1:5,000 dilution, as previously described (10, 11).

Western analysis of osteoclast and kidney lysates. Murine osteoclasts were used after *day 5* in culture for preparation of lysates. After two quick rinses with ice-cold phosphate-buffered saline (PBS), the cells were lysed in a buffer containing 10 mM Tris·HCl, pH 7.05, 50 mM NaCl, 0.5% Triton X-100, 30 mM sodium pyrophosphate, 5 mM NaF, 0.1 mM Na_3VnO_4, 5 mM $ZnCl_2$, and 2 mM PMSF. Lysates were pelleted by centrifugation at 15,000 rpm for 15 min at 4°C. The supernatant was transferred into a fresh microfuge tube and held on ice. Protein concentrations were measured using the Bio-Rad protein assay reagent kit (Bio-Rad) so that equal amounts of protein were loaded per lane (5–50 μg) and analyzed by SDS-PAGE on 8% gels. Western blot analyses were done as previously described (10, 11). The gel was then electroblotted onto a PVDF membrane by wet-dry transfer (Enprotech, Integrated Separation Systems). Nonspecific protein binding was blocked with 5% nonfat dry milk powder dissolved in PBS containing 0.1% Tween 20. The blots were incubated overnight with a 1:5,000 dilution of the primary antibody to the Npt2a cotransporter. This was followed by detection with a horseradish peroxidase (HRP)-conjugated secondary goat anti-rabbit antibody (Sigma; 1:1,000 dilution). The secondary antibody (HRP-conjugated goat anti-rabbit antibody) was detected by the enhanced chemiluminescence (ECL) detection kit (Amersham Biosciences, Piscataway, NJ) following the manufacturer's instructions, and as previously described (10, 11).

Transient transfection of murine osteoclasts with EGFP-Npt2a-WT and Npt2a-ΔTRL. For transfection of osteoclasts, the osteoclast culture medium was replaced with serum-free (SF) MEM medium (SF-MEM). Approximately 0.8 μg of each DNA (EGFP-Npt2a-WT/-Npt2a-ΔTRL) was used to transfect the cells with the transfection reagent Lipofectamine 2000 (Life Technologies) following the manufacturer's instructions. The DNA and Lipofectamine reagent complex was then added to the osteoclasts, and the plates were rocked gently before incubation for 4 h at 37°C, 5% CO_2. After the incubation, the SF-MEM medium was replaced with 10% serum-containing MEM (α-10 MEM) and incubated for 48 h at 37°C, 5% CO_2. These osteoclasts were then fixed and processed for immunostaining, as detailed below.

RT-PCR in the osteoclast and screening of cDNA library for PiT-1. Primers for amplification of murine PiT-1 were as follows: forward, 5′-CACCCATATGGCTTCTGCTT-3′, and reverse, 5′-CAGGAATTCATAGCCCAGGA-3′. The primers were chosen from the murine (kidney) PiT-1 sequence (GenBank accession no. M73696). The PCR reactions were performed using cDNA templates from RT reactions performed with equal quantities of total RNA isolated from murine osteoclasts and rat kidneys. The conditions for PCR-amplification of PiT-1 were as follows: an initial denaturation at 94°C for 4 min, followed by 35 cycles of 94°C for 1 min, annealing at 50°C for 1 min, and extension at 72°C for 1 min. A final extension was done for 10 min at 72°C. Two cDNA libraries (100 ng of template) were screened for PiT-1, one from rabbit osteoclasts (28), and the other from murine macrophages (Stratagene), using the same primer pairs and PCR conditions mentioned above. The expected size of the PiT-1 amplicons was 600 bp, which was subsequently confirmed by sequencing.

In situ hybridization of PiT-1 in the murine osteoclast. In situ hybridization for PiT-1 mRNA in osteoclasts was performed, as previously described (27). Murine osteoclasts were seeded on coverslips. The cells were washed in diethyl pyrocarbonate (DEPC)-PBS and fixed in 4% paraformaldehyde at room temperature for 20 min. The osteoclasts were permeabilized with 0.3% Triton X-100 for 15 min at room temperature. After the cells were rinsed in PBS, they were treated with proteinase K (5 μg/ml) for 30 min at 37°C. To inactivate proteinase K, the osteoclasts were rinsed for 5 min at room temperature in 0.1 M glycine and PBS. The endogenous peroxidase was inhibited with 2% H_2O_2 in PBS for 30 min at room temperature. The osteoclasts were post fixed in 4% paraformaldehyde for 20 min at room temperature and acetylated for 5 min at room temperature with 0.25% acetic anhydride in 0.1 M triethanolamine (pH 8.0). Subsequently, the cells were rinsed with DEPC water and prehybridized at 48°C for 2 h in a humidified chamber. At the end of prehybridization, the osteoclasts were incubated successively with 50, 70, 95, and 100% ethanol; the dehydrated cells were denatured with 50% formamide solution in 2× SSC for 10 min at 60°C and air-dried briefly. The cells were incubated overnight at 48°C with hybridization solution (50% form-

amide, 5× Denhardt's, 0.5 M NaCl, 50 mM dibasic sodium phosphate, 5 mM EDTA, 10 mM DTT, 0.5% SDS, 1% milk powder, and 0.1 mg/ml salmon sperm DNA) solution, containing heat denatured digoxigenin sense and antisense PiT-1 probes (2.5 ng/μl) under humidified conditions. A separate set of osteoclasts was incubated with hybridization solution without any probes to serve as negative control. The cells were then washed in 2× SSC for 5 min and with STE (500 mM NaCl, 1 mM EDTA and 20 mM Tris-Cl, pH 7.5) for 1 min at room temperature. The osteoclasts were washed with 50% formamide in 2× SSC for 30 min at room temperature. The cells were then placed in *buffer 1* (100 mM maleic acid, 100 mM NaCl, and 0.3% Triton X-100, pH 7.5) for 5 min and blocked with *buffer 1* containing 10% normal horse serum for 1 h at room temperature. For antibody visualization of digoxigenin, the osteoclasts were further incubated with anti-digoxigenin alkaline phosphatase-conjugated antibody (diluted 1:500) in blocking solution at 4°C overnight in a humidified chamber. These cells were rinsed successively in *buffer 1* and *buffer 3* (100 mM Tris, 100 mM NaCl, and 50 mM $MgCl_2$, pH 9.5). To each of the wells containing osteoclasts on the coverslips, 1 ml of NBT-BCIP (Roche Diagnostics) staining solution (that was prepared just before use) was added and incubated overnight at room temperature in the dark. After 24 h, cells were washed in DEPC-PBS, mounted, and visualized using a Nikon E800 microscope equipped with a SPOT camera (Diagnostic Instruments, Alexandria, VA).

Construction of the retroviral vector encoding for PiT-1. PiT-1 was tagged at the carboxy terminus by subcloning PiT-1 cDNA into the pSC2-HA plasmid containing a double HA epitope tag (YPYDVPDYA), derived from influenza hemagglutinin (6). Using PCR mutagenesis, a segment of PiT-1 cDNA was amplified using primers 5′-CCATGGCAATATGTGGCATGCC-3′ (sense) and 5′-CAAACAGAGCTCCATTCTGAGGATGACC-3′ (antisense), resulting in the removal of the stop codon and the introduction of a *Sac*I site (underlined). The modified PiT-1 cDNA was subcloned into the pSC2-HA plasmid between *Hin*dIII and *Sac*I in the same reading frame as the HA tag. The HA-tagged PiT-1 cDNA was then digested with *Hin*dIII and *Stu*I and subcloned into the retroviral vector pLNSX between *Hind*III and *Cla*I, which was filled in using T4 DNA polymerase to create the pLNSPiT1-HA plasmid. Vector particles were produced, as previously described (8).

Immunostaining of osteoclast cultures. Murine osteoclasts were rinsed twice in ice-cold PBS, fixed with 3% paraformaldehyde, and permeabilized with PBS containing 0.2% Triton X-100. The cells were blocked with PBS containing 2% bovine serum albumin (BSA) overnight. The cells were incubated for 2 h in a 1:500 dilution of the primary antibody at room temperature in the blocking solution described above. In experiments to determine the cellular distribution of NHERF-1 and Npt2a, NHERF-1 was detected with a chicken (IgY) polyclonal antibody, whereas Npt2a was detected with a rabbit (IgG) polyclonal COOH-terminal antibody. After two 15-min rinses with PBS containing 0.1% Tween 20, the cells were further incubated with rhodamine phalloidin (Sigma) to stain the actin cytoskeleton, as previously described (10, 11). The transfected pool of Npt2a was detected by fluorescence of EGFP. Epifluorescence was detected with either a Nikon Eclipse 800 microscope equipped with a SPOT camera (Diagnostic Instruments, Alexandria, VA) or a Bio-Rad Radiance 2100 confocal microscope. Confocal microscopy (Bio-Rad Radiance 2100) for immunostaining of Npt2a and NHERF-1 was performed with an Alexa-568-conjugated goat anti-rabbit antibody and Alexa-488-conjugated goat anti-chicken antibody (Molecular Probes), respectively. All images shown were taken with a Plan Apo ×60/1.4 na oil-immersion objective lens. The lateral (*xy*) resolution at this magnification was 0.12–0.17 μm.

RESULTS

Validation of Npt2a protein expression in normal mouse osteoclasts. We have previously demonstrated that an Npt2a-like protein was present in the osteoclast, which was either closely related or identical to that in the kidney (10, 11). In the current study, we have definitively established the identity of the Npt2a protein in the osteoclast by Western analysis of osteoclast lysates isolated from *Npt2a*+/+ and *Npt2a*−/− mice. Using a COOH-terminal antibody to Npt2a, we detected an 88-kDa protein in osteoclast lysates from *Npt2a*+/+ but not in *Npt2a*−/− mice (Fig. 1*A*, *lanes 1* and *2*; ~80 μg protein/lane). As controls for the Western blots, murine kidney homogenates (~25 μg protein/lane) were isolated from *Npt2a*+/+ and *Npt2a*−/− mice (Fig. 1*B*, *lanes 1* and *2*). As expected, there was no detectable signal in *Npt2a*−/− mice. The individual Western blots for Npt2a in osteoclast and kidney lysates were reprobed for actin to demonstrate protein loading for each lane.

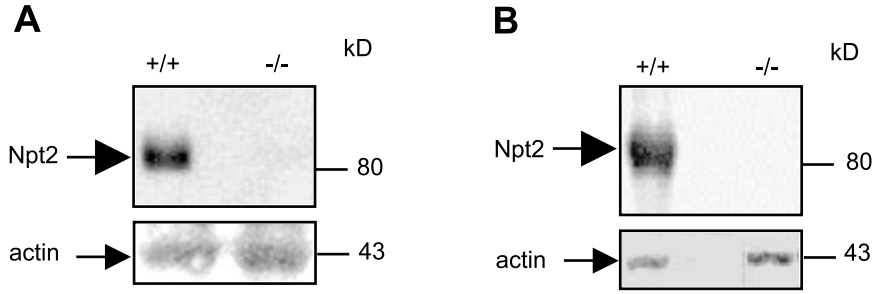

Fig. 1. Validation of type IIa Na/phosphate (P_i) cotransporter (Npt2a) protein expression in normal murine osteoclasts. *A*: murine osteoclast (mOC) lysates from Npt2a-wild type (+/+, 80 μg protein) and null mice (−/−, 80 μg protein) were immunoblotted with an antibody toward the COOH terminus of Npt2a. Lower panel shows the corresponding immunoblot for actin to demonstrate equal protein loading. *B*: murine kidney homogenates from Npt2a-wild type (+/+, 25 μg protein) and null mice (−/−, 25 μg protein) were probed with the antibody toward the COOH terminus of Npt2a. Lower panel shows the corresponding immunoblot for actin to demonstrate equal protein loading.

Cellular distribution of Npt2a, actin, and NHERF-1 in the osteoclast. We previously showed that Npt2a is localized almost exclusively on the basolateral membrane, near the sealing zone of the polarized osteoclast on bone (10, 11). In the present study, we examined the nature of the association of Npt2a with the actin cytoskeleton. Murine osteoclasts, cultured on glass, were immunostained for Npt2a (FITC, green), while actin was stained with rhodamine phalloidin (red). The localization of Npt2a is contiguous to the actin cytoskeleton, as shown in Fig. 2*A*. Significant colocalization of Npt2a with the actin ring near the periphery of the osteoclast was evident, as indicated in yellow. NHERF-1 is associated with various membrane transporters (31) and is generally classified as a membrane-cytoskeletal adaptor protein. We showed that NHERF-1 can be readily detected in the murine osteoclast by Western blotting (Fig. 2*B*, *lane 2*) using a previously characterized polyclonal antibody to NHERF-1 (30). We used rat kidney homogenates (Fig. 2*B*, *lane 1*) as a positive control for the Western blot. The NHERF-1 antibody recognizes an ~50-kDa protein in several species, including rat, human, and mouse (25, 30).

We then examined the cellular distribution of NHERF-1 in the murine osteoclast. In the representative confocal image of the osteoclast that was immunostained for NHERF-1, at least 13 nuclei can be seen, distributed toward the periphery. NHERF-1 was found to be localized predominantly at or near the plasma membrane, with some perinuclear staining, as shown (Fig. 2*C*). We next examined the possibility that the cellular distribution of Npt2a is contiguous or colocalized with that of NHERF-1 in the polarized osteoclast. For this purpose, we performed immunofluorescence in murine osteoclasts plated on 1-μm $CaPO_4$-coated Osteologic discs, a substrate on which osteoclasts are polarized, as previously described (10). Both NHERF-1 (Fig. 2*Da*) and Npt2a (Fig. 2*Db*) proteins colocalized near the periphery of the osteoclast (Fig. 2*Dc*).

Confocal microscopy was used to examine the cellular distribution of Npt2a and NHERF-1 in the osteoclast in more detail (Fig. 2*E*, *a*–*c*). As shown, NHERF-1 is localized primarily at the osteoclast plasma membrane (Fig. 2*Ea*). A similar cellular distribution pattern was obtained for Npt2a (Fig. 2*Eb*), and, given the limits of the confocal optics (i.e., the lateral resolution at this magnification was 0.12–0.17 μm), the two pro-

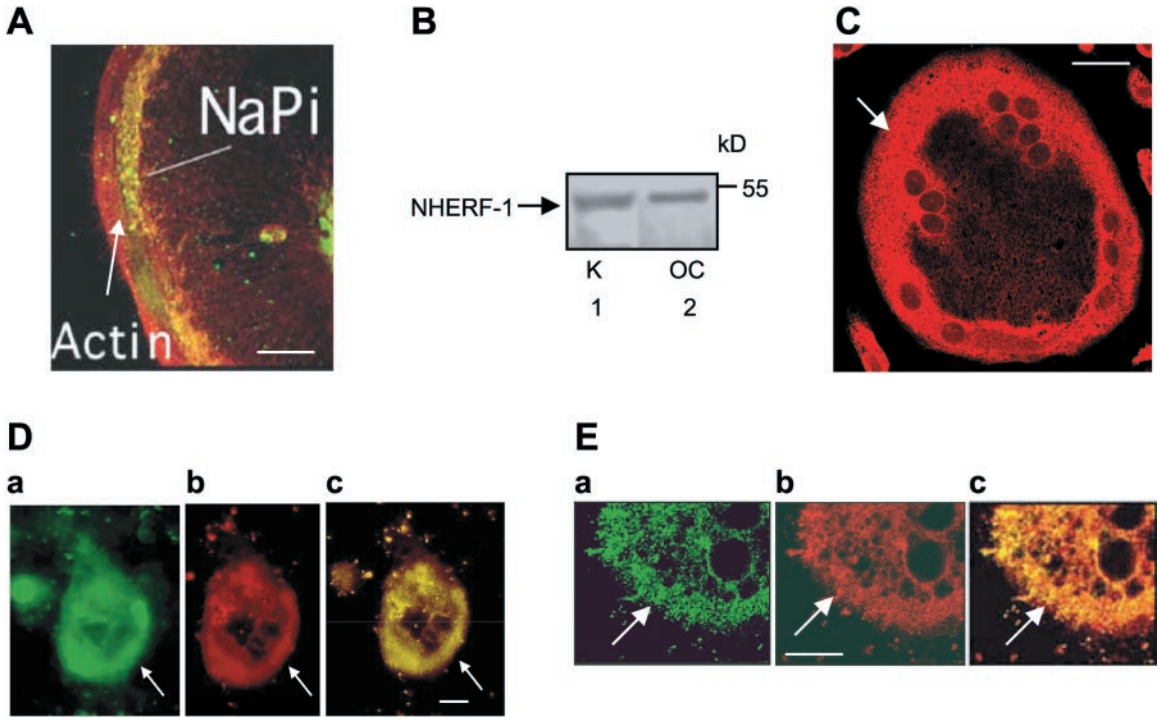

Fig. 2. Cellular distribution and expression of Npt2a, actin, and Na/H exchanger regulatory factor (NHERF-1) in the osteoclast. *A*: murine osteoclasts cultured on glass coverslips were immunostained for Npt2a (green); actin was stained with rhodamine phalloidin (red). The arrow points to the actin ring; colocalization of Npt2a and actin is indicated by line on the right. *B*: rat kidney homogenates (K, 25 μg, *lane 1*) and murine osteoclast lysates (OC, 50 μg, *lane 2*) were Western blotted for NHERF-1. *C*: cellular distribution of NHERF-1 in the murine osteoclast, as assessed by confocal microscopy. Multiple nuclei (~13) in this osteoclast can be seen distributed toward the periphery. Magnification shown is ×60. Scale bar represents 20 μm. *D*: cellular distribution of NHERF-1 (*a*) with Npt2a (*b*) in the osteoclast. The merged image for peripheral colocalization of NHERF-1 and Npt2a is shown in yellow (*c*). Scale bar represents 10 μm. *E*: colocalization of Npt2a (*a*) with NHERF-1 (*b*), using confocal microscopy. The merged image for Npt2a and NHERF-1 is indicated by punctate staining at the plasma membrane (*c*). Magnification shown is ×60. Scale bar represents 20 μm. Results shown are representative of 3–4 similar experiments.

teins colocalized in a punctate manner at the osteoclast plasma membrane, with additional diffuse central/perinuclear staining (Fig. 2*Ec*).

Interaction of NHERF-1 with Npt2a: affinity-precipitation assays. Having established that Npt2a and NHERF-1 are present in the osteoclast, we examined whether Npt2a associates with the adaptor protein. NHERF-1 was produced as a GST fusion protein and incubated with murine osteoclast lysates, and the affinity precipitates with GST-NHERF-1 were Western blotted for Npt2a. The signal for Npt2a in murine osteoclast lysates is shown (Fig. 3*A*, *lane 1*); there was no signal obtained for Npt2a when the GST protein itself was incubated with murine osteoclast lysates (Fig. 3*A*, *lane 2*). The Npt2a protein could be detected when rat kidney lysates were incubated with GST-NHERF-1 (Fig. 3*A*, *lane 3*). A signal for Npt2a was also detected when murine osteoclast lysates were incubated with the GST-NHERF-1 fusion protein (Fig. 3*A*, *lane 4*). These findings were further corroborated using

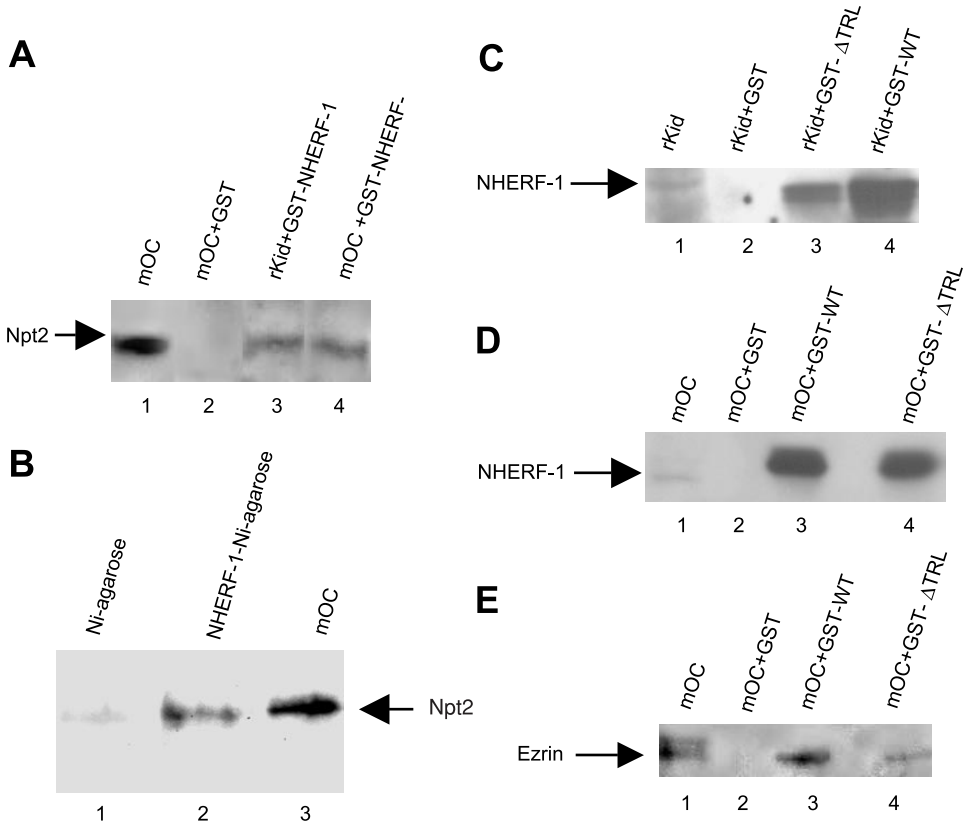

Fig. 3. Interaction of Npt2a with NHERF-1. *A*: glutathione *S*-transferase (GST)-NHERF-1 was used for affinity-precipitation of Npt2a in rat kidney homogenates (rKid, ~100 μg) and murine osteoclast lysates (mOC, ~500 μg). *Lane 1*: Western blot for Npt2a obtained from murine osteoclast lysates (mOC, ~50 μg); *lane 2*: as a negative control, GST protein itself was incubated with murine osteoclast lysates (mOC + GST). Signal for Npt2a in the GST-NHERF-1 affinity-precipitation from rat kidney homogenates (rKid + GST-NHERF-1, *lane 3*) and signal for Npt2a when murine osteoclast lysates were incubated with the GST-NHERF-1 fusion protein (mOC + GST-NHERF-1, *lane 4*) are shown. *B*: murine osteoclast lysates were used for affinity-precipitation of Npt2a with nickel (Ni)-agarose-NHERF-1. Npt2a was detected by Western blotting. *Lane 1*: negative control in the absence of the 6XHis-tagged NHERF-1 fusion protein (Ni-agarose). *Lane 2*: signal for murine osteoclast lysates incubated with NHERF-1-Ni-agarose beads (NHERF-1-Ni-agarose). *Lane 3*: signal for Npt2a in total murine osteoclast lysates as positive control (mOC). *C*: GST-Npt2a fusion proteins were used for affinity-precipitation of NHERF-1 from rat kidney homogenates. NHERF-1 was detected by Western blotting. The GST-Npt2a fusion proteins encoded either the wild-type (WT) COOH-terminal fragment of Npt2a (Npt2a-WT, COOH-terminal 82 amino acids) or the truncated COOH-terminal fragment of Npt2a where the TRL motif was deleted (Npt2a-ΔTRL, COOH-terminal 79 amino acids). *Lane 1*: Western blot for NHERF-1 as positive control (rKid); *lane 2*: negative control for affinity-precipitation of NHERF-1 (rKid + GST); *lane 3*: affinity-precipitation of NHERF-1 (rKid + GST-Npt2a-ΔTRL); and *lane 4*: affinity-precipitation of NHERF-1 (rKid + GST-Npt2a-WT). *D*: GST-Npt2a-WT or GST-Npt2a-ΔTRL fusion proteins were used for affinity-precipitation of NHERF-1 from murine osteoclast lysates. NHERF-1 was detected by Western blotting. *Lane 1*: Western blot for NHERF-1 as positive control (mOC); *lane 2*: negative control for affinity-precipitation of NHERF-1 (mOC + GST); *lane 3*: affinity-precipitation of NHERF-1 (mOC + GST-Npt2a-WT); and *lane 4*: affinity-precipitation of NHERF-1 (mOC + GST-Npt2a-ΔTRL). *E*: affinity-precipitation of ezrin with GST-Npt2a fusion proteins in osteoclasts. The immunoblots from affinity-precipitation of NHERF-1 with GST-Npt2a-WT or -ΔTRL fusion proteins (in *D*) were stripped and reprobed with a monoclonal antibody to ezrin. *Lane 1*: Western blot for ezrin (mOC); *lane 2*: negative control (mOC + GST); *lane 3*: affinity-precipitation of ezrin (mOC + GST-Npt2a-WT); and *lane 4*: affinity-precipitation of ezrin (mOC + GST-ΔTRL). Results shown are representative of 3 similar experiments.

6XHis-tagged NHERF-1 bound to Ni-agarose beads and incubated with murine osteoclast lysates (Fig. 3*B*). In the absence of 6XHis-tagged NHERF-1, there was very little binding of Npt2a to Ni-agarose (Fig. 3*B*, *lane 1*); however, Npt2a was bound to the 6XHis-tagged NHERF-1 (Fig. 3*B*, *lane 2*). The signal for Npt2a in the osteoclast lysates is also shown (Fig. 3*B*, *lane 3*). Taken together, these experiments suggest an association of Npt2a with NHERF-1 in the osteoclast.

The association of Npt2a with NHERF-1 has been localized to the carboxy terminus of Npt2a, which has a TRL motif, as previously reported (9). Yeast two-hybrid assays had shown that the interaction of Npt2a with NHERF-1 is abrogated when the PDZ-binding motif was deleted. To examine whether this COOH-terminal PDZ-binding motif was indeed critical in the association of Npt2a with NHERF-1, we performed in vitro GST affinity-precipitation assays using either the WT COOH-terminal fragment of Npt2a or the truncated COOH terminus fragment of Npt2a where the TRL motif was deleted. First, rat kidney homogenates (rKiD) were incubated with the GST-Npt2a-WT and GST-Npt2a-ΔTRL fusion proteins; the affinity precipitates were Western blotted with the NHERF-1 antibody. The signal for NHERF-1 can be detected in rat kidney homogenates (Fig. 3*C*, *lane 1*); there was no detectable signal for NHERF-1 when the GST protein alone was incubated with rat kidney homogenates (Fig. 3*C*, *lane 2*). However, NHERF-1 could be detected with both the GST-Npt2a-ΔTRL (Fig. 3*C*, *lane 3*) and GST-Npt2a-WT (Fig. 3*C*, *lane 4*), although the levels of NHERF-1 associated with the GST-Npt2a-ΔTRL fusion protein were far less compared with that precipitated with the GST-Npt2a-WT fusion protein. Therefore, these GST affinity-precipitation studies show that although the COOH-terminal TRL motif of Npt2a is important for binding NHERF-1 in the kidney, the interaction of Npt2a with NHERF-1 is not completely lost in the absence of the PDZ motif.

Next, we performed similar GST affinity-precipitation studies using murine osteoclasts. Murine osteoclast lysates were incubated with the GST-Npt2a-WT and GST-Npt2a-ΔTRL fusion proteins; these affinity precipitates were probed with the NHERF-1 antibody. Our results are summarized as follows in Fig. 3*D*, *lanes 1–4*. The signal for NHERF-1 can be detected in osteoclast lysates (Fig. 3*D*, *lane 1*); there was no discernible signal for NHERF-1 when the GST protein alone was incubated with murine osteoclast lysates (Fig. 3*Cb*, *lane 2*). NHERF-1 could be detected with both the GST-Npt2a-WT (Fig. 3*D*, *lane 3*) and GST-Npt2a-ΔTRL (Fig. 3*D*, *lane 4*). However, the levels of NHERF-1 associated with the GST-Npt2a-ΔTRL fusion protein were only slightly reduced compared with that of the GST-Npt2a-WT fusion protein, in contrast to our findings in the kidney. This suggests that although the Npt2a protein in the osteoclast is identical or closely related to that in the kidney, its binding affinity to NHERF-1 may differ from that in the kidney.

The ezrin-radixin-moesin (ERM)-complex is known to mediate the interaction between NHERF-1 and actin (1). We hypothesized that ezrin would comprise a link between Npt2a-NHERF-1 and actin in the osteoclast. To examine this possibility, the immunoblots for the GST-Npt2a-NHERF-1 affinity-precipitations (Fig. 3*D*) were stripped and reprobed with a monoclonal antibody to ezrin (Fig. 3*E*, *lanes 1–4*). The signal for ezrin can be seen at ~80 kDa in murine osteoclast lysates, as shown in Fig. 3*E*, *lane 1*. When murine osteoclast lysates were incubated with GST protein alone, ezrin did not coprecipitate (Fig. 3*E*, *lane 2*). Ezrin was readily detectable when murine osteoclast lysates were incubated with GST-Npt2a-WT fusion protein (Fig. 3*E*, *lane 3*). The levels of ezrin that were detectable in affinity precipitates with GST-Npt2a-ΔTRL fusion protein were noticeably lower compared with that obtained with the GST-Npt2a-WT fusion protein (Fig. 3*E*, *lane 4*). The likely explanation for these findings is that NHERF-1 binds ezrin directly and that the association of Npt2a with ezrin is indirectly mediated by NHERF-1.

Cellular distribution of Npt2a-WT and Npt2a-ΔTRL in murine osteoclasts. NHERF-1 has been implicated in the membrane sorting of several transporters (26). We next asked whether there were any differences in sorting of the Npt2a-WT and Npt2a-ΔTRL proteins in the osteoclast. Although osteoclasts are notorious for being resistant to conventional methods of transfection, transfection can be achieved in a small percentage of cells in culture (18). First, we plated murine osteoclasts on glass coverslips, which were then transfected with either the Npt2a-WT or the Npt2a-ΔTRL constructs in an EGFP vector, as shown in Fig. 4*A*, *lanes 1–3*. As a control for the EGFP-derived fluorescence, murine osteoclasts were also transfected with the empty EGFP vector. The osteoclasts were subsequently processed for EGFP-derived immunofluorescence 48 h later. As shown in the EGFP-control cells, there was a low level of diffuse fluorescence due to the EGFP alone (Fig. 4*A*, *lane 1*). In osteoclasts that were transfected with EGFP-Npt2a-WT, the cellular distribution of EGFP-Npt2a was seen as both perinuclear and peripheral near the plasma membrane, as indicated by the arrow (Fig. 4*A*, *lane 2*). In contrast, the cellular distribution of EGFP-Npt2a-ΔTRL was apparent as mostly perinuclear and weak staining at the plasma membrane, as indicated by the arrow (Fig. 4*A*, *lane 3*).

We next examined the cellular distribution of the EGFP-Npt2a-WT and EGFP-Npt2a-ΔTRL proteins in osteoclasts that were actively involved in resorption by confocal microscopy. When murine osteoclasts are plated on 1-μm-thick $CaPO_4$-coated quartz discs, the matrix is actively resorbed and the resorbed areas can be visualized as clear areas on the quartz disc, as shown in Fig. 4*B*. On this substrate, murine osteoclasts can form multiple actin rings within one cell, which are normally associated with resorption centers (10). Murine osteoclasts plated on $CaPO_4$-coated quartz discs were transfected with either EGFP-Npt2a-WT or EGFP-Npt2a-ΔTRL and after 48 h were fixed and

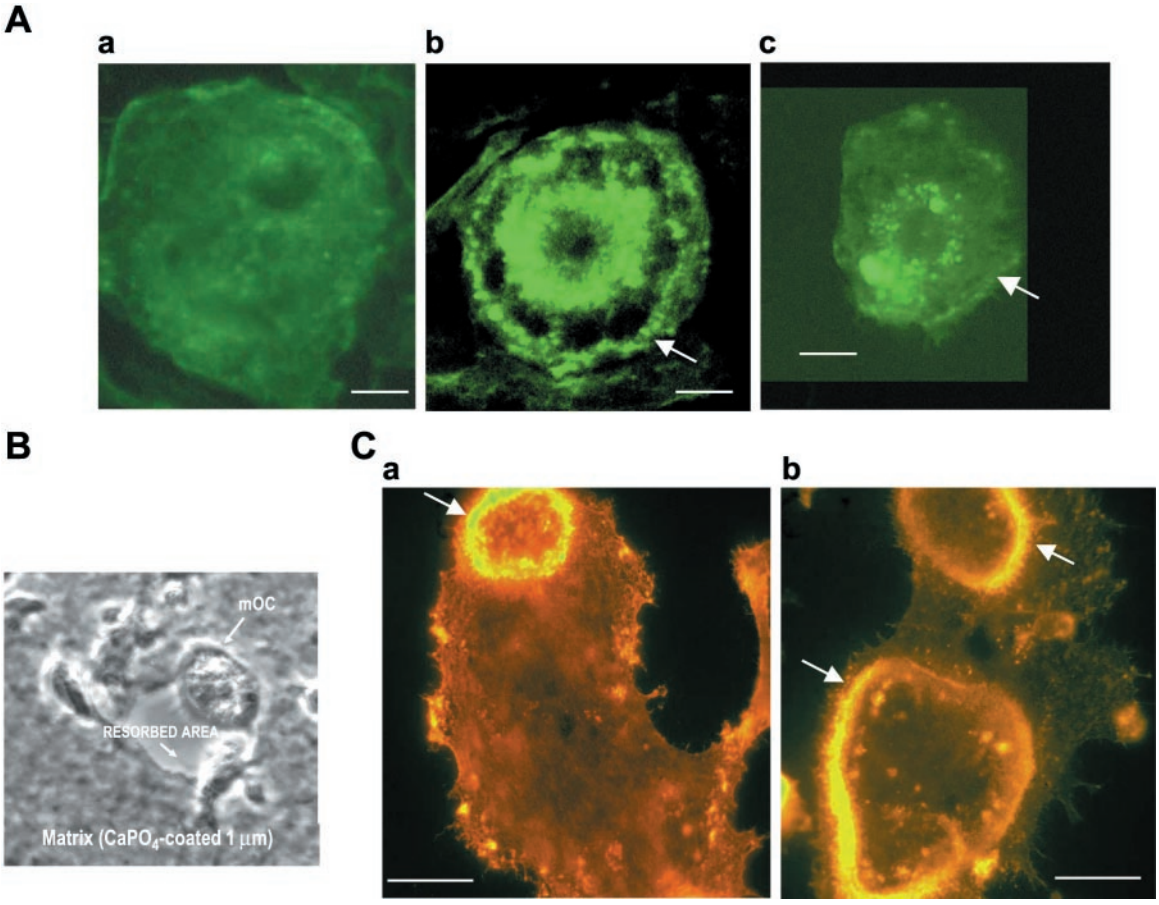

Fig. 4. *A*: sorting of Npt2a-WT and Npt2a-ΔTRL in the osteoclast. Murine osteoclasts were plated on glass coverslips and transfected with either the Npt2a-WT or the Npt2a-ΔTRL in an EGFP-vector. As a control, osteoclasts were transfected with the empty EGFP vector (*a*). The cellular distribution of EGFP-Npt2a-WT in osteoclasts (*b*); the arrow points to the EGFP-derived fluorescence at the plasma membrane. The cellular distribution of EGFP-Npt2a-ΔTRL in osteoclasts (*c*). The arrow points to the EGFP-derived fluorescence at the plasma membrane. Scale bar represents 20 μm. *B*: resorption by osteoclasts. Murine osteoclasts plated on 1-μm-thick $CaPO_4$-coated Osteologic (quartz) discs, where the matrix is actively resorbed. *C*: cellular distribution of actin and transfected EGFP-Npt2a-WT (*a*) or actin and EGFP-Npt2a-ΔTRL (*b*) in resorbing osteoclasts, as assessed by confocal microscopy. Colocalization of actin and EGFP-derived fluorescence is indicated in yellow and pointed to by the arrows. A Plan Apo ×60/1.4 na oil-immersion objective lens was used. Scale bar represents 20 μm. Figures are representative of 4–5 separate experiments.

stained for actin with rhodamine phalloidin. The signal for EGFP-Npt2a-WT was seen to colocalize with the actin ring, as indicated in yellow (Fig. 4*C*, *lane 1*). Using identical confocal settings, the signal EGFP-Npt2a-ΔTRL was also seen to colocalize with two actin rings, as shown within one representative osteoclast (Fig. 4*C*, *lane 2*). Although the fluorescence was not quantified, it was apparent that the intensity of the EGFP-Npt2a-ΔTRL signal that colocalized with actin was somewhat less than that for the corresponding EGFP-Npt2a-WT signal. In summary, these immunofluorescence data suggest that in spite of the absence of the COOH-terminal NHERF-1-binding TRL motif, Npt2a can still associate with actin in osteoclasts actively involved in resorption.

Expression of PiT-1 in osteoclasts. Previous studies demonstrated that hypophosphatemia in Npt2a knockout mice (*Npt2a*−/−) resulted in an age-dependent increase in type III Na/P_i cotransporter mRNA expression in the kidney as part of an effort to compensate for the loss of the *Npt2a* gene (12). Given the evidence that expression of other Na/P_i cotransporters can increase in the *Npt2a*−/− mice, we asked whether the type III family of Na/P_i cotransporters is expressed in the osteoclast. As previously mentioned, PiT-1 is one such galv receptor that is highly expressed in bone marrow, osteoblasts, and chondrocytes (19, 20, 22, 29). In our preliminary studies, we demonstrated the expression of PiT-1 in murine osteoclasts by RT-PCR, using total RNA isolated from murine osteoclasts, as shown in Fig. 5*A*, *lanes 1–4*. A 600-bp amplicon was obtained for both the murine osteoclast PiT-1 (Fig. 5*A*, *lane 2*) and the rat kidney PiT-1 (Fig. 5*A*, *lane 3*). In the absence of RT, no product was obtained from kidney RNA (Fig. 5*A*, *lane 4*). The sequence identity between the rat kidney and the murine osteoclast PiT-1 was 98%. Previously, we had successfully established the presence and identity of the Npt2a gene by PCR-based cloning of a rabbit

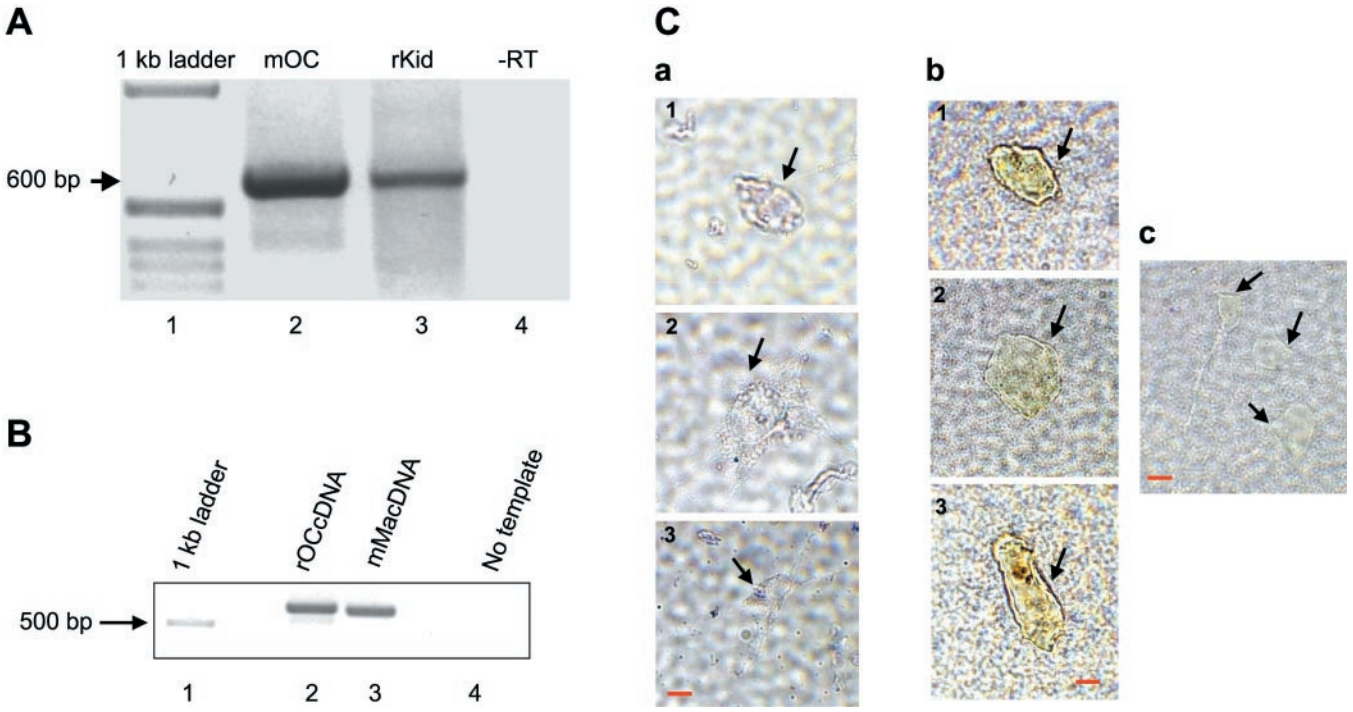

Fig. 5. Detection of PiT-1 transcript in the osteoclast. *A*: RT-PCR on RNA from osteoclasts. The transcript for PiT-1 was detected in murine osteoclasts (mOC) by RT-PCR, using primers from conserved sequences between the murine and rat kidney (rKid) PiT-1 variants. A 1-kb DNA ladder was used to estimate size of the amplicons (*lane 1*); a 600-bp amplicon was obtained for PiT-1 in the murine osteoclast (mOC, *lane 2*) and rat kidney (rKid, *lane 3*); negative control for RT-PCR is shown (−RT, l*ane 4*). *B*: PCR-based screening in an osteoclast cDNA library. A rabbit osteoclast (rOC) and a murine macrophage (mMa) cDNA library were separately screened for PiT-1. The 1-kb DNA ladder was used to estimate size of the amplicons (*lane 1*); a 600-bp amplicon (rOC cDNA, *lane 2*) and murine macrophages (mMa cDNA, *lane 3*) were detected; negative control is shown (i.e., no cDNA template, *lane 4*). *C*: in situ hybridization for PiT-1 mRNA in the osteoclast. Murine osteoclasts (mOCs) hybridized with sense digoxigenin-labeled riboprobes for PiT-1 (*a*, *1–3*), mOCs hybridized with antisense digoxigenin-labeled riboprobes for PiT-1 (*b*, *1–3*), and mOCs that were not hybridized with either sense or antisense riboprobes for PiT-1 served as negative controls (c) are shown. Magnification shown is with a ×63 oil-immersion lens.

osteoclast and a mouse macrophage cDNA library (10, 11). In the current study, to further establish the presence of PiT-1 in osteoclasts, we detected PiT-1 by PCR-screening of the cDNA library generated from rabbit osteoclasts (rOC cDNA), as shown (Fig. 5*B*, *lane 2*); PiT-1 could also be detected in a murine macrophage cDNA library (Fig. 5*B*, *lane 3*). There was no detectable signal for PiT-1 in the absence of cDNA template (Fig. 5*B*, *lane 4*). Therefore, these data suggest that both the osteoclast and the macrophage express the PiT-1 transporter. To prove that the RT-PCR signal for PiT-1 was indeed originating from osteoclastic cells, we decided to perform in situ hybridization for PiT-1 in murine osteoclasts in culture. No signal was detected in osteoclasts hybridized with sense digoxigenin-labeled riboprobes for PiT-1 (Fig. 5*A*, *lanes 1–3*). However, a signal was detected in osteoclasts hybridized with antisense digoxigenin-labeled riboprobes for PiT-1, as shown in the brown-yellow color (Fig. 5*B*, *lanes 1–3*). Osteoclasts that were not hybridized with either sense or antisense riboprobes for PiT-1 served as negative controls (Fig. 5*C*). Therefore, our in situ results, combined with those obtained from RT-PCR and PCR-based amplification of PiT-1 from (osteoclast and macrophage) cDNA libraries, suggest that PiT-1 is expressed in the osteoclast and osteoclast-like cells.

Cellular distribution of PiT-1 in osteoclasts. Currently, there are no antibodies available for PiT-1. To circumvent this limitation, we infected murine osteoclasts with a retroviral vector carrying a replication-deficient retrovirus that contains a HA-tagged PiT-1 cDNA, as shown in Fig. 6*A*. This provides a high-efficiency gene transfer of a HA-tagged PiT-1 into osteoclasts. Murine osteoclasts plated on glass coverslips were assayed for immunofluorescence 48 h postinfection with the retrovirus. Actin was labeled with rhodamine phalloidin, whereas PiT-1 immunofluorescence was detected using an HA antibody. As can be seen, the punctate cellular distribution of PiT-1 is contiguous to that of actin, at or near the plasma membrane, as indicated in yellow. Similar results were obtained with two different dilutions of the retrovirus encoding for PiT-1 (1:1,000 and 1:500). Next, murine osteoclasts were plated on 1-μm-thick $CaPO_4$-coated Osteologic discs, as previously described (10). Osteoclasts become polarized and avidly resorb the matrix (10). Murine osteoclasts were infected with the retrovirus-encoded HA-tagged PiT-1 for 48 h. PiT-1 was seen to colocalize

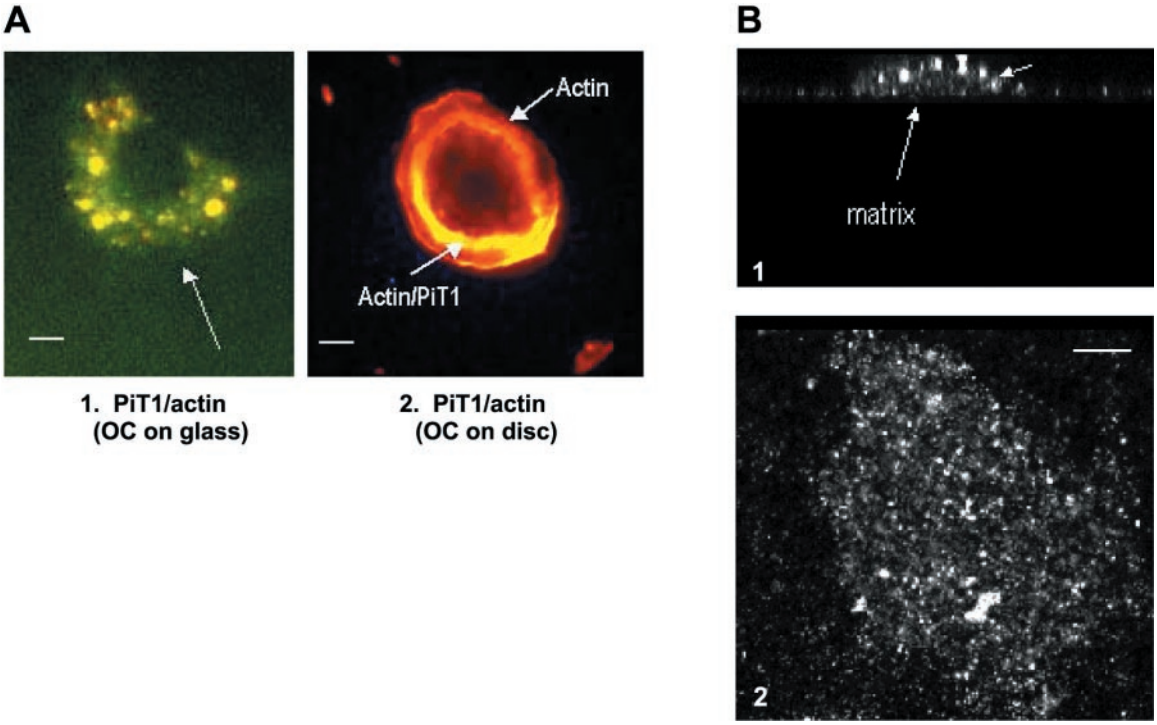

Fig. 6. Cellular distribution of PiT-1 in the osteoclast. Murine osteoclasts were plated either on glass coverslips (where they are unpolarized) or on resorbable $CaPO_4$-coated matrices (where they are polarized). These osteoclasts were infected with a retroviral vector carrying a replication-deficient retrovirus that contained a HA-tagged PiT-1 cDNA. Actin was labeled with rhodamine phalloidin, and PiT-1 immunofluorescence was detected using an HA antibody. *A*: PiT-1 in unpolarized osteoclasts. Scale bar represents 10 μm. *B*: PiT-1 in polarized osteoclasts. Scale bar represents 20 μm. *C*: basolateral localization of PiT-1. *1*: cross-sectional (*xz*) view of the polarized osteoclast and distribution of PiT-1, using confocal microscopy. The top arrow points to the basolateral membrane, whereas the bottom arrow points to the matrix. A planar optical section of the basolateral membrane of the osteoclast is also shown (*2*). Scale bar represents 20 μm.

with the actin ring, as shown in the representative osteoclast (Fig. 6*B*). Next, we used confocal microscopy to assess the polarity of the PiT-1 distribution, as shown in an *xz* (cross section) view of the osteoclast (Fig. 6*C*, *lane 1*). The transporter was found to localize almost exclusively to the basolateral membrane and the sealing zone, similar to that previously reported for the Npt2a cotransporter. The planar optical section that was used to generate the cross-sectional view of the osteoclast is shown (Fig. 6*C*, *lane 2*). The cellular distribution of PiT-1 is punctate on the basolateral surface of the polarized osteoclast.

DISCUSSION

We previously demonstrated that an Npt2a-like Na/P_i cotransporter is expressed in the osteoclast and is exclusively localized to the basolateral membrane of the polarized osteoclast (10, 11). In addition, we showed that phosphonoformic acid, a selective inhibitor of Na/P_i cotransport, greatly diminished the resorptive capacity of osteoclasts and that disruption of the actin cytoskeleton in osteoclasts greatly diminished Na-dependent P_i uptake (10).

In the present study, we demonstrate that Npt2a protein in the osteoclast is identical to that in the kidney as previously suggested (10, 11) and is absent from Npt2a-null osteoclasts. We also demonstrate, using GST-fusion protein affinity-precipitation assays, that the Npt2a protein in the osteoclast interacts with the PDZ-domain protein NHERF-1. Previous studies using the yeast two-hybrid system indicated that the TRL motif of Npt2a is critical for binding to NHERF-1 as well as other PDZ-domain proteins in the kidney (9). Some of these PDZ proteins are localized in the brush border or in the subapical compartment of proximal tubular cells. These proteins include NaP_i-Cap1 and NaP_i-Cap2, identical to diphor-1 and PDZK1 (16, 17). It has been suggested that because PDZ proteins also interact with the actin cytoskeleton, they contribute to the stabilization of proteins at or near the plasma membrane (26).

The yeast two-hybrid studies also suggested that removal of the COOH-terminal amino acid residues, TRL, blunted the interaction of the Npt2a cotransporter with NaP_i-Cap1, NaP_i-Cap2, NHERF-1, and NHERF-2 (9). This conclusion was based on the lack of β-galactosidase activation by the TRL-truncated COOH-terminal tail of Npt2a; however, no GST affinity-precipitation assays were performed with either the full-length or the truncated Npt2a construct. In our studies, we subcloned fragments of the Npt2a cDNA that spanned 82 amino acids from the COOH terminus (the GST-Npt2a-WT fusion protein), or 79 amino acids that lacked the terminal TRL domain at the COOH

terminus (the GST-Npt2a-ΔTRL fusion protein). Our in vitro GST affinity-precipitation studies indicate that the TRL motif in Npt2a is not the sole determinant for binding to NHERF-1, either in the kidney or in the osteoclast. Using rat kidney homogenates, we found that when the PDZ-binding motif was deleted, NHERF-1 was still recovered, although the recovery was far less than that with the WT Npt2a protein, consistent with our recent demonstration that the COOH-terminal TRL motif of Npt2a is not the sole determinant of apical membrane expression in polarized opossum kidney (OK) cells (13). An upstream proline-arginine ($P_{578}R_{579}$) sequence appeared to play an additional role in membrane expression of the Npt2a protein (13). Our affinity-precipitation studies using the GST-Npt2a-WT and GST-Npt2a-ΔTRL fusion proteins contain the upstream PR sequence, which may explain the finding that Npt2a lacking the COOH-terminal TRL motif can still bind NHERF-1. It is of interest, however, that nearly identical findings have been found using similar Npt2a fusion proteins in affinity-precipitation assays in a renal epithelial cell line, suggesting that NHERF-1 and Npt2a may bind at more than one site (Lederer ED and Weinman EJ, unpublished observations). Moreover, a similar paradigm may also characterize the interaction between NHERF-1 and NHE3 (Weinman EJ, unpublished observations). The nature of the putative alternate site or sites of interaction between NHERF-1 and Npt2a remains to be determined.

We have shown that Npt2a associates indirectly with ezrin in the osteoclast, a finding that may explain the indirect association with the actin cytoskeleton. In the kidney, NHERF-1 is predominantly found in brush-border membranes, with a minor fraction in the basolateral membrane and in the cytosol (30). These separate pools of NHERF-1 have been hypothesized to shuttle between the different membrane domains to regulate ion transport. NHERF-1 associates with an NH_2-terminal ezrin/radixin/moesin domain (ERMAD), conserved in proteins that belong to the ERM family of actin-binding proteins, serving as a membrane-cytoskeleton bridge; several studies have suggested that various transporters are linked to the actin cytoskeleton through the NHERF-1-ERM complex (26). This association between NHERF and the ERM complex may determine the membrane sorting of Npt2a in the osteoclast. We found some discernible differences in the sorting of the Npt2a-WT and the Npt2a-ΔTRL proteins in the osteoclast, as seen from our immunofluorescence studies. In actively resorbing osteoclasts, multiple actin rings were seen to form, which delineated areas of resorptive activity. There was a redistribution of the Npt2a (WT and ΔTRL) protein, from the plasma membrane to these actin rings. However, in nonresorbing osteoclasts (plated on glass), our immunofluorescence data indicate that the plasma membrane localization of the Npt2a-WT protein is more intense than that of Npt2a-ΔTRL. This observation is consistent with findings in opossum kidney (OK) cells, where the TRL-truncated Npt2a cotransporter was still partially expressed at the apical membrane, although part of it was detected inside the cell (13). Indeed, an upstream sequence (i.e., $P_{578}R_{579}$) is also involved in apical expression of the cotransporters (13). Mutation of this PR motif, or removal of all downstream residues, resulted in almost a total loss of apical membrane expression of Npt2a in OK cells. It was suggested that there was an "unmasking" of this internal PR motif after removal of several amino acid residues upstream of the COOH-terminal TRL motif. The question remains whether the internal PR sequence functions as a sorting signal or as an anchoring determinant for Npt2a in the osteoclast or the kidney. Future studies, using either adenoviral or retroviral vectors for high-efficiency gene transfer, will permit a more in-depth investigation of the activity and sorting behavior of Npt2a-WT and the Npt2a-ΔTRL proteins. Furthermore, the application of pulse chase and surface biotinylation strategies will facilitate the study of Npt2a half-life and membrane sorting in osteoclasts and kidney derived from NHERF-1 null mice (25).

We have previously reported that the hypophosphatemia in young *Npt2a−/−* mice is associated with skeletal abnormalities and a mild osteoclast defect (11). The absence of a more flagrant osteopetrotic phenotype in *Npt2a−/−* mice suggested that other P_i transport mechanism(s) in the osteoclast compensate(s) for the deficiency of Npt2a. We have hypothesized that the type III family of Na/P_i cotransporters may adapt to the lack of the Npt2a protein in osteoclasts (11). In the present study we demonstrate that PiT-1, a member of the type III family of Na/P_i cotransporters, is expressed in the murine osteoclast. This was accomplished by RT-PCR of RNA isolated from osteoclasts in culture and PCR-based screening of an osteoclast cDNA library. Moreover, our preliminary data show that PiT-1 in the osteoclast is probably identical to that found in the kidney.

We have also demonstrated that PiT-1 is localized to the basolateral membrane of the polarized osteoclast and that its distribution in the osteoclast is similar to what we previously reported for Npt2a (10). Moreover, the colocalization of PiT-1 with actin in the polarized osteoclast is consistent with the plasma membrane localization of PiT-1. It is of interest that the receptor for amphotropic murine leukemia viruses, PiT-2, has been reported to associate with actin in CHO cells (24). The colocalization of PiT-2 with actin in these cells can be modified by variations in concentration of extracellular P_i (24). On the basis of these findings, it was postulated that changes in the actin cytoskeleton (such as formation of stress fibers) may be responsible for conformational changes in PiT-2 that in turn determine its activity as a P_i transporter. Although PiT-1 does not contain any recognizable PDZ-binding motifs that may mediate an indirect association with actin, the activity of PiT-1 in the osteoclast in response to ambient P_i levels may be linked to changes in the osteoclast actin network that occur during attachment to bone matrix and subsequent resorption. Future studies are necessary to assess the relative contribu-

tion of PiT-1 to osteoclast function in both WT and *Npt2a*−/− mice.

This work was supported by National Institute of Arthritis and Musculoskeletal and Skin Diseases Grant AR-44706 and a Designated Research Initiatives Fund Grant from the University of Maryland, Baltimore, MD, to A. Gupta, National Institute of Arthritis and Musculoskeletal and Skin Diseases Grant AR-46292 to M. A. Chellaiah, and National Institute of Diabetes and Digestive and Kidney Diseases Grant DK-55881 and a Department of Veterans Affairs Research Service grant to E. J. Weinman. H. S. Tenenhouse and H. Murer were supported by grants from the Canadian Institutes for Health Research (FRN 44355) and the Swiss National Science Foundation (31.46523 and 31.6539), respectively.

REFERENCES

1. **Algrain M, Turunen O, Vaheri A, Louvard D, and Arpin M.** Ezrin contains cytoskeleton and membrane binding domains accounting for its proposed role as a membrane-cytoskeletal linker. *J Cell Biol* 120: 129–139, 1993.
2. **Anderson HC.** Normal and abnormal mineralization in mammals. *Trans Am Soc Artif Intern Organs* 27: 702–708, 1981.
3. **Beck L, Karaplis AC, Amizuka N, Hewson AS, Ozawa H, and Tenenhouse HS.** Targeted inactivation of *Npt2* in mice leads to severe renal phosphate wasting, hypercalciuria, and skeletal abnormalities. *Proc Natl Acad Sci USA* 95: 5372–5377, 1998.
4. **Chellaiah M, Kizer N, Silva M, Alvarez U, Kwiatkowski D, and Hruska KA.** Gelsolin deficiency blocks podosome assembly and produces increased bone mass and strength. *J Cell Biol* 148: 665–678, 2000.
5. **Chellaiah MA, Biswas RS, Yuen D, Alvarez UM, and Hruska KA.** Phosphatidylinositol 3,4,5-trisphosphate directs association of Src homology 2-containing signaling proteins with gelsolin. *J Biol Chem* 276: 47434–47444, 2001.
6. **Chen CM, Kraut N, Groudine M, and Weintraub H.** I-mf, a novel myogenic repressor, interacts with members of the MyoD family. *Cell* 86: 731–741, 1996.
7. **Fanning AS and Anderson JM.** PDZ domains: fundamental building blocks in the organization of protein complexes at the plasma membrane. *J Clin Invest* 103: 767–772, 1999.
8. **Farrell KB, Ting YT, and Eiden MV.** Fusion-defective gibbon ape leukemia virus vectors can be rescued by homologous but not heterologous soluble envelope proteins. *J Virol* 76: 4267–4274, 2002.
9. **Gisler SM, Stagljar I, Traebert M, Bacic D, Biber J, and Murer H.** Interaction of the type IIa Na/P_i cotransporter with PDZ proteins. *J Biol Chem* 276: 9206–9213, 2001.
10. **Gupta A, Guo XL, Alvarez UM, and Hruska KA.** Regulation of sodium-dependent phosphate transport in osteoclasts. *J Clin Invest* 100: 538–549, 1997.
11. **Gupta A, Tenenhouse HS, Hoag HM, Wang D, Khadeer MA, Namba N, Feng X, and Hruska KA.** Identification of the type II Na^+-P_i cotransporter (Npt2) in the osteoclast and the skeletal phenotype of Npt2−/− mice. *Bone* 29: 467–476, 2001.
12. **Hoag HM, Martel J, Gauthier C, and Tenenhouse HS.** Effects of Npt2 gene ablation and low-phosphate diet on renal Na^+/phosphate cotransport and cotransporter gene expression. *J Clin Invest* 104: 679–686, 1999.
13. **Karim-Jimenez Z, Hernando N, Biber J, and Murer H.** Molecular determinants for apical expression of the renal type IIa Na^+/P_i-cotransporter. *Pflügers Arch* 442: 782–790, 2001.
14. **Kavanaugh MP and Kabat D.** Identification and characterization of a widely expressed phosphate transporter/retrovirus receptor family. *Kidney Int* 49: 959–963, 1996.
15. **Kavanaugh MP, Miller DG, Zhang W, Law W, Kozak SL, Kabat D, and Miller AD.** Cell-surface receptors for gibbon ape leukemia virus and amphotropic murine retrovirus are inducible sodium-dependent phosphate symporters. *Proc Natl Acad Sci USA* 91: 7071–7075, 1994.
16. **Kocher O, Comella N, Gilchrist A, Pal R, Tognazzi K, Brown LF, and Knoll JH.** PDZK1, a novel PDZ domain-containing protein up-regulated in carcinomas and mapped to chromosome 1q21, interacts with cMOAT (MRP2), the multidrug resistance-associated protein. *Lab Invest* 79: 1161–1170, 1999.
17. **Kocher O, Comella N, Tognazzi K, and Brown LF.** Identification and partial characterization of PDZK1: a novel protein containing PDZ interaction domains. *Lab Invest* 78: 117–125, 1998.
18. **Kojima H, Nemoto A, Uemura T, Honma R, Ogura M, and Liu YY.** rDRAK1, a novel kinase related to apoptosis, is strongly expressed in active osteoclasts and induces apoptosis. *J Biol Chem* 276: 19238–19243, 2001.
19. **O'Hara B, Johann SV, Klinger HP, Blair DG, Rubinson H, Dunn KJ, Sass P, Vitek SM, and Robins T.** Characterization of a human gene conferring sensitivity to infection by gibbon ape leukemia virus. *Cell Growth Differ* 1: 119–127, 1990.
20. **Palmer G, Bonjour JP, and Caverzasio J.** Expression of a newly identified phosphate transporter/retrovirus receptor in human SaOS-2 osteoblast-like cells and its regulation by insulin-like growth factor I. *Endocrinology* 138: 5202–5209, 1997.
21. **Palmer G, Guicheux J, Bonjour JP, and Caverzasio J.** Transforming growth factor-β stimulates inorganic phosphate transport and expression of the type III phosphate transporter Glvr-1 in chondrogenic ATDC5 cells. *Endocrinology* 141: 2236–2243, 2000.
22. **Palmer G, Manen D, Bonjour JP, and Caverzasio J.** Characterization of the human Glvr-1 phosphate transporter/retrovirus receptor gene and promoter region. *Gene* 226: 25–33, 1999.
23. **Palmer G, Zhao J, Bonjour J, Hofstetter W, and Caverzasio J.** In vivo expression of transcripts encoding the Glvr-1 phosphate transporter/retrovirus receptor during bone development. *Bone* 24: 1–7, 1999.
24. **Rodrigues P and Heard JM.** Modulation of phosphate uptake and amphotropic murine leukemia virus entry by posttranslational modifications of PIT-2. *J Virol* 73: 3789–3799, 1999.
25. **Shenolikar S, Voltz JW, Minkoff CM, Wade JB, and Weinman EJ.** Targeted disruption of the mouse NHERF-1 gene promotes internalization of proximal tubule sodium-phosphate cotransporter type IIa and renal phosphate wasting. *Proc Natl Acad Sci USA* 99: 11470–11475, 2002.
26. **Shenolikar S and Weinman EJ.** NHERF: targeting and trafficking membrane proteins. *Am J Physiol Renal Physiol* 280: F389–F395, 2001.
27. **Tenenhouse HS, Roy S, Martel J, and Gauthier C.** Differential expression, abundance, and regulation of Na^+-phosphate cotransporter genes in murine kidney. *Am J Physiol Renal Physiol* 275: F527–F534, 1998.
28. **Tezuka K, Tezuka Y, Maejima A, Sato T, Nemoto K, Kamioka H, Hakeda Y, and Kumegawa M.** Molecular cloning of a possible cysteine proteinase predominantly expressed in osteoclasts. *J Biol Chem* 269: 1106–1109, 1994.
29. **Van Zeijl M, Johann SV, Closs E, Cunningham J, Eddy R, Shows TB, and O'Hara B.** A human amphotropic retrovirus receptor is a second member of the gibbon ape leukemia virus receptor family. *Proc Natl Acad Sci USA* 91: 1168–1172, 1994.
30. **Wade JB, Welling PA, Donowitz M, Shenolikar S, and Weinman EJ.** Differential renal distribution of NHERF isoforms and their colocalization with NHE3, ezrin, and ROMK. *Am J Physiol Cell Physiol* 280: C192–C198, 2001.
31. **Weinman EJ, Steplock D, Tate K, Hall RA, Spurney RF, and Shenolikar S.** Structure-function of recombinant Na/H exchanger regulatory factor (NHE-RF). *J Clin Invest* 101: 2199–2206, 1998.